BIOCHEMISTRY
including biophysical chemistry & molecular biology
Article

Biochemistry **2010,** *49,* 6165–6176 6165
DOI: 10.1021/bi100503w

Human DNA Ligase III Recognizes DNA Ends by Dynamic Switching between Two DNA-Bound States[†,‡]

Elizabeth Cotner-Gohara,[§,#] In-Kwon Kim,[§,#] Michal Hammel,[∥] John A. Tainer,[⊥,▽] Alan E. Tomkinson,[@] and Tom Ellenberger*[,§]

[§]*Department of Biochemistry and Molecular Biophysics, Washington University School of Medicine, St. Louis, Missouri 63110,* [∥]*Physical Biosciences Division, Lawrence Berkeley National Laboratory, Berkeley, California 94720,* [⊥]*Life Sciences Division, Lawrence Berkeley National Laboratory, Berkeley, California 94720,* [▽]*Department of Molecular Biology and The Skaggs Institute for Chemical Biology, The Scripps Research Institute, La Jolla, California 92037, and* [@]*University of Maryland School of Medicine, Baltimore, Maryland 21201* [#]*These authors contributed equally to this work.*

Received April 2, 2010; Revised Manuscript Received May 14, 2010

ABSTRACT: Human DNA ligase III has essential functions in nuclear and mitochondrial DNA replication and repair and contains a PARP-like zinc finger (ZnF) that increases the extent of DNA nick joining and intermolecular DNA ligation, yet the bases for ligase III specificity and structural variation among human ligases are not understood. Here combined crystal structure and small-angle X-ray scattering results reveal dynamic switching between two nick-binding components of ligase III: the ZnF-DNA binding domain (DBD) forms a crescent-shaped surface used for DNA end recognition which switches to a ring formed by the nucleotidyl transferase (NTase) and OB-fold (OBD) domains for catalysis. Structural and mutational analyses indicate that high flexibility and distinct DNA binding domain features in ligase III assist both nick sensing and the transition from nick sensing by the ZnF to nick joining by the catalytic core. The collective results support a "jackknife model" in which the ZnF loads ligase III onto nicked DNA and conformational changes deliver DNA into the active site. This work has implications for the biological specificity of DNA ligases and functions of PARP-like zinc fingers.

DNA ligase III is a vertebrate-specific protein functioning in DNA replication and repair pathways, including nucleotide excision repair, base excision repair, and single-strand break repair, plus mitochondrial replication and repair (*1*). DNA ligase III is furthermore implicated in the repair of DNA double-strand breaks when nonhomologous end joining (NHEJ)[1] activity is compromised (*2*). Upregulated ligase III expression in chronic myeloid leukemia cells, with concomitant decreases in the level of expression of the NHEJ proteins DNA ligase IV and Artemis, may promote cell survival and disease progression, raising the possibility of selectively inhibiting ligase III as a cancer treatment (*3*). Besides repairing nuclear DNA, ligase III is the only mitochondrial DNA ligase in which it functions in DNA repair and replication.

Three DNA ligase III isoforms are generated by alternative mRNA splicing and translation initiation, and expression of one or more of these is essential for the viability of mammalian cells and animals (*4*). The LigIIIα isoform interacts with XRCC1 through a C-terminal BRCA1-related C-terminal (BRCT) domain, and this protein complex functions in a variety of DNA repair pathways, most prominently in the repair of DNA single-strand breaks (*5*, *6*). LigIII*β* lacks the C-terminal BRCT domain (*6*, *7*) and is expressed only in the male germ line where it presumably repairs DNA strand breaks during meiotic recombination (*7*, *8*). The mitochondrial DNA ligase III (mtLigIII) isoform has an N-terminal mitochondrial localization sequence besides the C-terminal BRCT interaction domain. However, XRCC1 is absent from mitochondria, and mtLigIII appears to function alone in mitochondrial DNA maintenance (*9*, *10*).

Besides LigIII, two other DNA ligases are expressed in mammalian cells. DNA ligase I (LigI) is an essential enzyme that repairs Okazaki fragments during DNA replication and also functions in long patch base excision repair. DNA ligase IV (LigIV) has specialized functions in the repair of DNA double-strand breaks by the NHEJ pathway, and in the rearrangement of immunoglobulin genes (*1*, *11*). All three mammalian DNA ligases contain a homologous catalytic core, consisting of two domains that are structurally conserved in prokaryotic DNA ligases and other members of a superfamily of nucleotidyl transferases that includes mRNA-capping enzymes and RNA

[†]This work was supported in part by National Institutes of Health (NIH) Grant 5R01 GM052504 (T.E.) and The Structural Cell Biology of DNA Repair Program (P01 CA92584 to A.E.T., T.E., and J.A.T.). Funding for the SIBYLS beamline was provided in part by the Offices of Science and Biological and Environmental Research, U.S. Department of Energy, under Contract DE-AC02-05CH11231. This work includes research conducted at the Northeastern Collaborative Access Team beamlines of the Advanced Photon Source, supported by Grant RR-15301 from the National Center for Research Resources at the National Institutes of Health. Use of the Advanced Photon Source is supported by the U.S. Department of Energy, Office of Basic Energy Sciences, under Contract DE-AC02-06CH11357.

[‡]Coordinates have been deposited with the Protein Data Bank as entry 3L2P.

*To whom correspondence should be addressed. Phone: (314) 362-0287. Fax: (314) 362-4432. E-mail: tome@biochem.wustl.edu.

[1]Abbreviations: LigIII, DNA ligase III; NTase, nucleotidyl transferase domain; OBD, oligonucleotide binding domain; DBD, DNA binding domain; ZnF, zinc finger domain; NHEJ, nonhomologous end joining; BRCT, BRCA1-related C-terminal domain; LigI, DNA ligase I; LigIV, DNA ligase IV; SAXS, small-angle X-ray scattering; PARP1, poly(ADP-ribose) polymerase I; rmsd, root-mean-square deviation.

Published on Web 06/02/2010

ligases (*12*). Additional N- and C-terminal regions flanking the catalytic core of mammalian DNA ligases provide other functions, including interactions with other proteins that dictate the subcellular localization of each enzyme. The nucleotidyl transferase (NTase) and OB-fold (OBD) domains comprise the catalytic core of DNA ligases that harbors essential residues participating in a three-step DNA end joining reaction (*1*). A third, noncatalytic domain located immediately N-terminal to the catalytic core of all three mammalian DNA ligases (*13*) extends the DNA interaction surface of these enzymes. This DNA binding domain (DBD) is essential for DNA recognition and nick joining functions of human LigI (*14*) and LigIII (*15*). A crystal structure of LigI bound to a nicked DNA revealed that the DBD and the adjoining NTase and OBD domains form a compact, ring-shaped structure that sequesters the ends of the nicked strand in the active site (*14*). At present, it is unknown if this protein architecture is conserved in the other mammalian DNA ligases and how structural modifications specific to each enzyme may contribute to their different biological functions.

In particular, the LigIII polypeptides are distinguished from the other human DNA ligases by the presence of an N-terminal zinc finger (ZnF) domain that binds cooperatively in conjunction with the adjacent DBD to nicks and gaps in the backbone of duplex DNA (*15*). This DNA nick sensing by the ZnF evidently contributes to substrate selection and increases the catalytic efficiency of nick joining by DNA ligase III (*15*−*18*). Furthermore, the ZnF has a profound effect on stimulating the intermolecular ligation of two DNAs (*15*), an activity likely relevant to the involvement of LigIIIα/XRCC1 in the back-up pathway of nonhomologous end joining (*2*). The DNA ligase III ZnF is structurally related to the two N-terminal zinc finger domains of poly(ADP-ribose) polymerase (*16*). Although a study of the LigIII ZnF domain by NMR identified residues in a β-hairpin motif that are strongly perturbed by the addition of DNA (*17*), the molecular mechanisms by which DNA nick sensing and catalytic activity are enhanced by the ZnF of LigIII are unknown.

To characterize the DNA interaction and structure of human ligase III, we combined X-ray crystal structural analysis with small-angle X-ray scattering (SAXS) to analyze solution architectures and flexibility. These experiments suggest how DNA ligase III interactions and conformational changes contribute to DNA substrate selection and end joining activities. This multidomain enzyme has a dynamic shape, permitting alternative ensembles of domains to engage the DNA in competing configurations. Conformational switching can assist in loading DNA ligase III onto nicked DNA and promoting the juxtaposition of two DNA molecules in the active site for ligation of two DNAs.

EXPERIMENTAL PROCEDURES

Protein Purification. LigIIIβ and ΔZnF-LigIII were purified as described previously (*15*), and purified protein was concentrated to 30−40 mg/mL and stored at −80 °C. Selenomethionine-labeled ΔZnF-LigIII protein was expressed in BL21(DE3) using amino acids to suppress methionine biosynthesis, as described previously (*19*), and was purified by the same protocol as the native protein. $LigIII_{755}$ (residues 1−755) and ΔZnF_{755} (residues 170−755) were cloned into pET28a and purified using the same protocols used for LigIIIβ and ΔZnF-LigIII, respectively.

Nicked DNA Substrate Preparation. The DNA strands were synthesized on an Applied Biosystems 394 DNA/RNA Synthesizer and were desalted using a SepPak cartridge (Waters, Inc.). The nicked DNA substrate was formed by annealing equimolar amounts of the three DNA strands [5′CGGGATGCGTddC (upstream; ddC is 2′,3′-dideoxycytidine monophosphate), 5′PO_4-GTCGGACTGGC (downstream), and 5′GCCAGTCCGAC-GACGCATCCCG (template)] in 5 mM MES (pH 6.5) and 20 mM NaCl.

Crystallization. A LigIII−DNA complex was formed by incubaton of 0.6 mM nicked DNA substrate, 0.6 mM ΔZnF-LigIIIβ, 1 mM ATP, and 10 mM $MgCl_2$. The ligase−DNA complex was mixed with an equal volume of well solution [1.8 M ammonium sulfate and 0.1 M sodium acetate (pH 5.6)]. Crystals ($P4_12_12$, a = 130.1 Å, b = 130.1 Å, and c = 150.4 Å) grew at 22 °C by hanging drop vapor diffusion. Prior to being flash-cooled in liquid nitrogen, crystals were washed in well solution and transferred to a cryoprotectant solution containing 1.8 M ammonium sulfate, 0.2 M sodium acetate (pH 5.6), and 25% glycerol. Crystals diffracted beyond 3.5 Å using synchrotron radiation, and there is one ΔZnF-LigIIIβ−DNA complex per asymmetric unit.

X-ray Data Collection. X-ray diffraction data extending to 3.0 Å resolution were collected from frozen crystals at the NE-CAT beamline at the Advanced Photon Source (Argonne, IL) and at the MBC beamline at the Advanced Light Source (Berkeley, CA). Data from two multiwavelength anomalous dispersion experiments and one native experiment were used. X-ray data were processed using HKL2000 (*20*) or d*trek and then scaled using Scalepack (*20*, *21*). Nineteen of 21 SeMet sites were located by automated Patterson searches using SOLVE (*22*). Heavy-atom parameters were refined, and experimental phases were calculated in SHARP using the native data set in combination with the MAD data sets (*23*). Experimentally phased maps had a well-defined solvent boundary and obvious electron density for both protein and nucleic acid. Phase improvement and density modification in SOLOMON in SHARP greatly enhanced the interpretability of the electron density. The binding register of the DNA with respect to the protein was determined using the clearly visible nick in the DNA backbone, and purines could be distinguished from pyrimidines. The SeMet sites, bulky amino acid side chains, and comparison to the DNA ligase I structure (*14*) helped define the amino acid register. The crystallographic model was constructed using COOT (*24*), with refinement in REFMAC (*25*). TLS parameters were refined using REFMAC, with the DBD, NTase, and OBD domains and DNA treated as separate domains. Figures were generated using PYMOL (www.pymol.org), and molecular surface electrostatics were calculated with APBS (*26*). Crystallographic data statistics are listed in Table 1.

Small-Angle X-ray Scattering. LigIII was adenylated with 5 mM $MgCl_2$ and 1 mM ATP for 1 h at 4 °C, and the reaction was quenched by addition of 10 mM EDTA. LigIII was dialyzed with a buffer containing 50 mM Tris-HCl (pH 7.5), 10% glycerol, 2 mM DTT, and 250 mM NaCl. For protein−DNA complexes, 20-mer nicked DNA substrate (3′-OH nick for LigIII without ZnF and 3′-ddC nick for LigIII with ZnF) was mixed with LigIII (protein:DNA ratio of 1:1.3), and all protein−DNA complexes were purified by gel filtration. However, comparison of purified and unpurified mixtures of LigIIIβ and DNA at different molar ratios (from 1:0.8 to 1:1.2) gave comparable although not identical results. LigIIIβ binds tightly to DNA in a buffer with 50 mM Tris-HCl (pH 7.5), 10% glycerol, 2 mM DTT, and 250 mM NaCl, while ΔZnF shows salt-dependent DNA binding affinity on gel filtration, which is consistent with the optimum

Table 1: Crystallographic Data Statistics[a]

			SeMet-2		
	native	SeMet-1	MAD[b] λ_1	MAD λ_2	MAD λ_3
beamline	NSLS 24-ID	NSLS 24-ID	ALS 4.2.2	ALS 4.2.2	ALS 4.2.2
wavelength (λ)	0.9791	0.9791	0.97911	0.97935	0.96412
resolution (Å)	3.0 (3.11−3.0)	3.15 (3.26−3.15)	3.1 (3.21−3.1)	3.11 (3.22−3.11)	3.2 (3.31−3.2)
completeness (%)	95.5 (73.5)	96.7 (79.2)	100 (100)	99.9 (100.0)	99.9 (100.0)
redundancy	12.9 (5.5)	5.3 (2.4)	7.11 (7.24)	7.12 (7.26)	7.16 (7.36)
R_{sym}[c]	0.057 (0.602)	0.094 (0.579)	0.145 (0.679)	0.144 (0.663)	0.2 (0.7)
$I/\sigma(I)$	25.0 (2.25)	11.2 (1.9)	6.9 (1.9)	6.9 (2.0)	5.6 (1.8)
phasing					
resolution (Å)	3.00	3.15	3.10	3.11	3.2
R_{cullis}[d] iso (cen/acen)/ano	0.825/0.839/−		−/−/0.844	0.721/0.693/0.885	0.810/0.792/0.962
phasing power[d] iso (cen/acen)/ano	0.0721/0.679/−		−/−/1.009	0.564/0.537/0.598	0.634/0.551/0.271
refinement					
resolution (Å)	3.00				
R_{cryst}/R_{free}[e]	0.235/0.271				
rmsd for bond lengths (Å)	0.016				
rmsd for bond angles (deg)	1.840				

[a]Statistics reported in parentheses represent data for the highest-resolution shell. [b]Multiwavelength anomalous dispersion (MAD) X-ray data statistics from one wavelength (λ) of a three-λ MAD experiment. [c]$R_{sym} = \sum|I - \langle I\rangle|/\sum\langle I\rangle$, where I is the reflection intensity and $\langle I\rangle$ is the average intensity of multiple symmetry-related reflections. [d]As reported by SHARP. [e]$R_{cryst} = \sum|F_o - F_c|/\sum|F_o|$, where F_o and F_c are the observed and calculated structure factor amplitudes, respectively. R_{free} was calculated with a test set of reflections (5% of the data).

near 100 mM NaCl for nick joining and DNA binding activities of ΔZnF (*15*, *16*). Thus, LigIIIβ/LigIII$_{755}$−DNA complexes were purified at 250 mM NaCl to protect them from aggregation, whereas ΔZnF/ΔZnF$_{755}$−DNA complexes were purified at 100 mM NaCl.

SAXS data were collected at ALS beamline 12.3.1 LBNL (Berkeley, CA) (*27*). Incident X-rays were tuned to a wavelength (λ) of 1.0−1.5 Å at a sample-to-detector distance of 1.5 m, resulting in scattering vectors (q) ranging from 0.007 to 0.31 Å^{-1}. The scattering vector is defined as $q = 4\pi \sin\theta/\lambda$, where 2θ is the scattering angle. All experiments were performed at 20 °C, and data were processed as described previously (*27*). Briefly, the data were acquired at short and long time exposures (0.5 and 5 s, respectively) and then scaled and merged for calculations using the entire scattering spectrum. The experimental SAXS data were evaluated for aggregation by inspection of Guinier plots (*28*). The radius of gyration R_g was derived by the Guinier approximation $I(q) = I(0)\exp(-q^2R_g^2/3)$ with the limits $qR_g < 1.6$. GNOM (*29*) was used to compute the pair distance distribution functions, $P(r)$. This approach also provided the maximum dimension of the macromolecule, D_{max}. In our rigid-body modeling strategy BILBOMD, molecular dynamics simulations were used to explore conformational space adopted by LigIIIβ constructs. A minimal ensemble search (MES) is used to identify the minimal set of conformers required to accurately fit the experimental data (*30*). For more details about data evaluation, see the Supporting Information.

Site-Directed Mutagenesis and Mutant Purification. LigIIIβ was mutated using the Quickchange site-directed mutagenesis kit (Stratagene), and mutant proteins were expressed in *Escherichia coli* Rosetta cells. Cells were grown in LB medium containing ampicillin at 37 °C, and cultures were induced with 1 mM isopropyl thiogalactoside at 16 °C. After being incubated for 16 h, cells were harvested. Cells were resuspended in buffer A [50 mM Tris-HCl (pH 7.5), 150 mM NaCl, 0.2% NP-40, 5 mM β-mercaptoethanol, 1 mM PMSF, 1 mM benzamidine-HCl, 1 μg/mL aprotinin, 2 μg/mL leupeptin, 1 μg/mL pepstatin A, and 1 μg/mL chymostatin] and lysed by sonication. The lysate was clarified by centrifugation at 30,000*g* for 1 h at 4 °C and loaded onto a phosphocellulose column equilibrated with buffer A. The fraction eluted with buffer A with 1 M NaCl was pooled and loaded onto a 5 mL HiTrap nickel chelating column (GE Healthcare) equilibrated with buffer B [50 mM Tris-HCl (pH 7.5), 250 mM NaCl, 5 mM β-mercaptoethanol, 1 mM PMSF, and 1 mM benzamidine-HCl]. Following a wash with buffer B, the mutant proteins were eluted stepwise with buffer B and 50 and 500 mM imidazole. Freshly purified protein was concentrated and used for the ligation assay.

DNA End Joining Assays. DNA ligation activities with nicked and blunt-ended DNA substrates were measured at 22 °C as described previously (*15*). For ligation of an RNA−DNA heteroduplex containing a single-strand nick, the downstream (15-mer) RNA oligonucleotide was 5′-labeled with polynucleotide kinase. RNA-containing substrates were reacted with full-length LigIIIβ at 4 or 22 °C, and DNA-containing substrates were reacted at 4 °C for different periods of time. Reactions were quenched by addition of 10 mM EDTA with formamide. The RNA oligonucleotide (15-mer), adenylated intermediate, and ligation product (28-mer) were separated by denaturing PAGE and quantified with a phosphorimaging device (GE Healthcare Typhoone).

RESULTS

Structural Organization of DNA Ligase III in a Complex with DNA. To define the molecular structure of LigIII and its DNA interactions, we crystallized the LigIII catalytic region comprising the DBD, NTase, and OBD domains (ΔZnF-LigIIIβ protein) in complex with a 22-mer nicked DNA substrate (Figure 1). The enzyme was captured prior to step 2 of the ligation reaction with the AMP cofactor covalently bonded to Lys421 in the active site (Figure S1 of the Supporting Information). The protein architecture and conformation of ΔZnF-LigIIIβ engaging nicked DNA resemble those of human LigI bound to nicked DNA (*14*), despite only 21% amino acid sequence identity. The three domains (DBD, NTase, and OBD) completely encircle the DNA and sequester the 3′-OH and 5′-PO$_4$

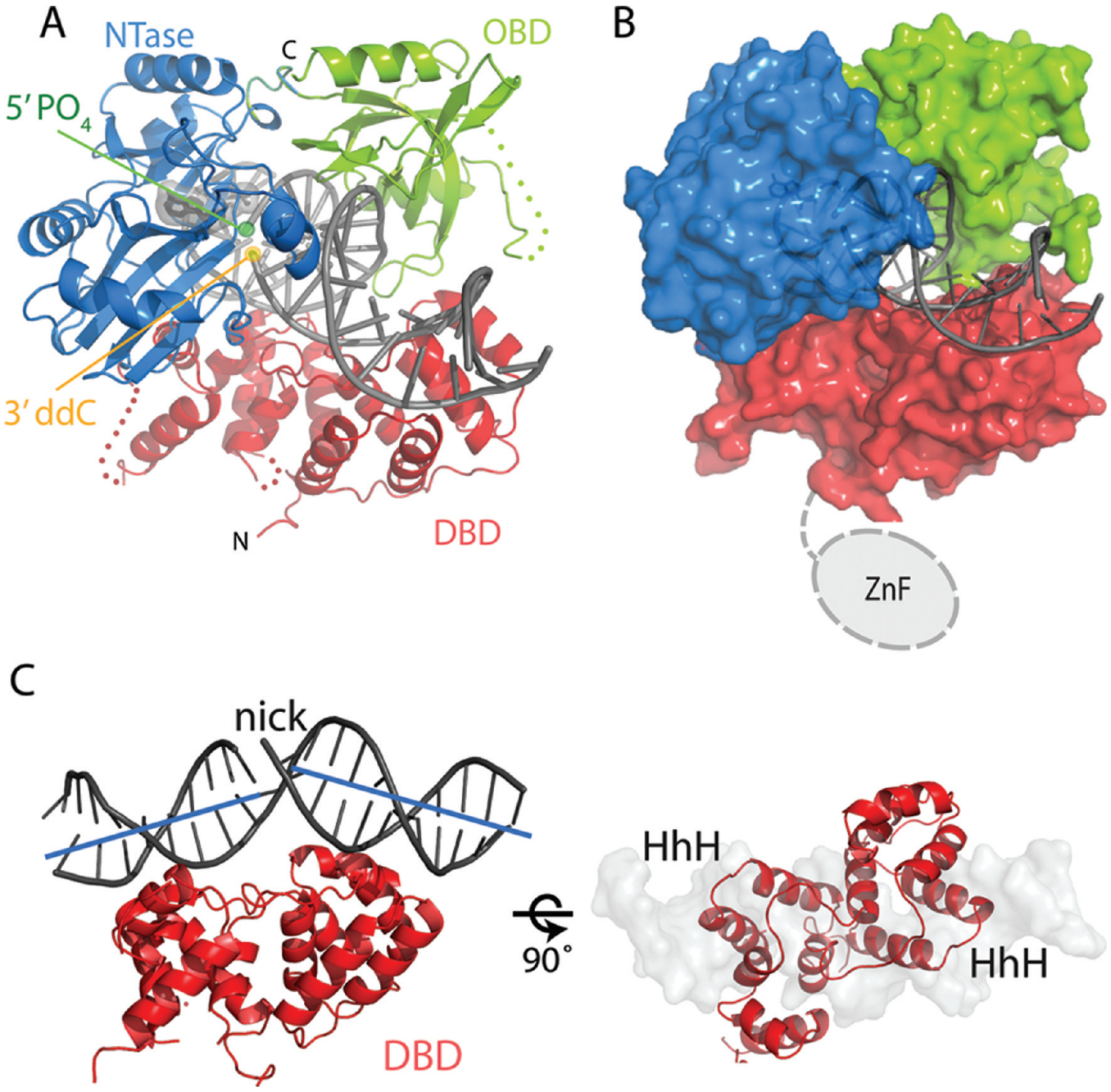

FIGURE 1: Structure of ΔZnF-LigIIIβ bound to DNA. (A) Ligase III bound to a nicked DNA substrate. The adenylated ΔZnF-LigIIIβ protein was captured in a pre-step 2 complex with DNA prior to the transfer of AMP to the DNA. The 5′-PO_4 and 3′-ddC termini of the nicked DNA strand are highlighted in green and yellow, respectively. The crystallographic model contains 537 residues of the 697-residue protein fragment that was crystallized and 43 of the 44 nucleotides. The 100 C-terminal amino acids (residues 747−862) are disordered, indicating that this region is flexible. However, comparison to ligase homologues indicates that the entire OBD domain is observed. In addition, there are three disordered loops in the protein: two in the DNA-binding domain (DBD, residues 207−213 and 376−383) and one in the OB-fold domain (OBD, residues 666−691). All three of these loops are located on the exterior of the protein, away from the DNA and domain interfaces. (B) Surface view of ΔZnF-LigIIIβ bound to DNA showing that ligase III forms a continuous ring about the DNA during step 2 with the nicked DNA strand sequestered in the active site pocket of the NTase domain. (C) DBD of ligase III forming a platform for the highly distorted DNA, which is partially unwound and has an offset in the helical axis about the nick (left). The DBD interacts with the DNA through two helix−hairpin−helix motifs that insert into the minor groove on either side of the nick (*45*).

termini of the nicked DNA strand. On the basis of this new structure, a clamplike structure is a hallmark of eukaryotic DNA ligases bound to their DNA substrates (*14*, *31*, *32*) that is mimicked by ligases from lower organisms (*14*, *31*, *32*). The enclosed architecture of the enzyme−substrate complex may serve to orient the ends of two DNA strands for ligation. The LigIII NTase domain primarily engages the nicked DNA strand, whereas the OBD domain inserts into the minor groove of the DNA duplex opposite the nick, helping to secure the bound DNA within the active site of the NTase domain (Figure S2 of the Supporting Information). A comparison of the crystal structures of human DNA ligase III and ligase I shows conserved residues within the NTase and OBD domains that interact with and stabilize the DNA in an underwound conformation, thereby exposing the ends of the nicked strand to the enzyme active site (Figure 1C) (*14*). The similarities between the pre-step 2

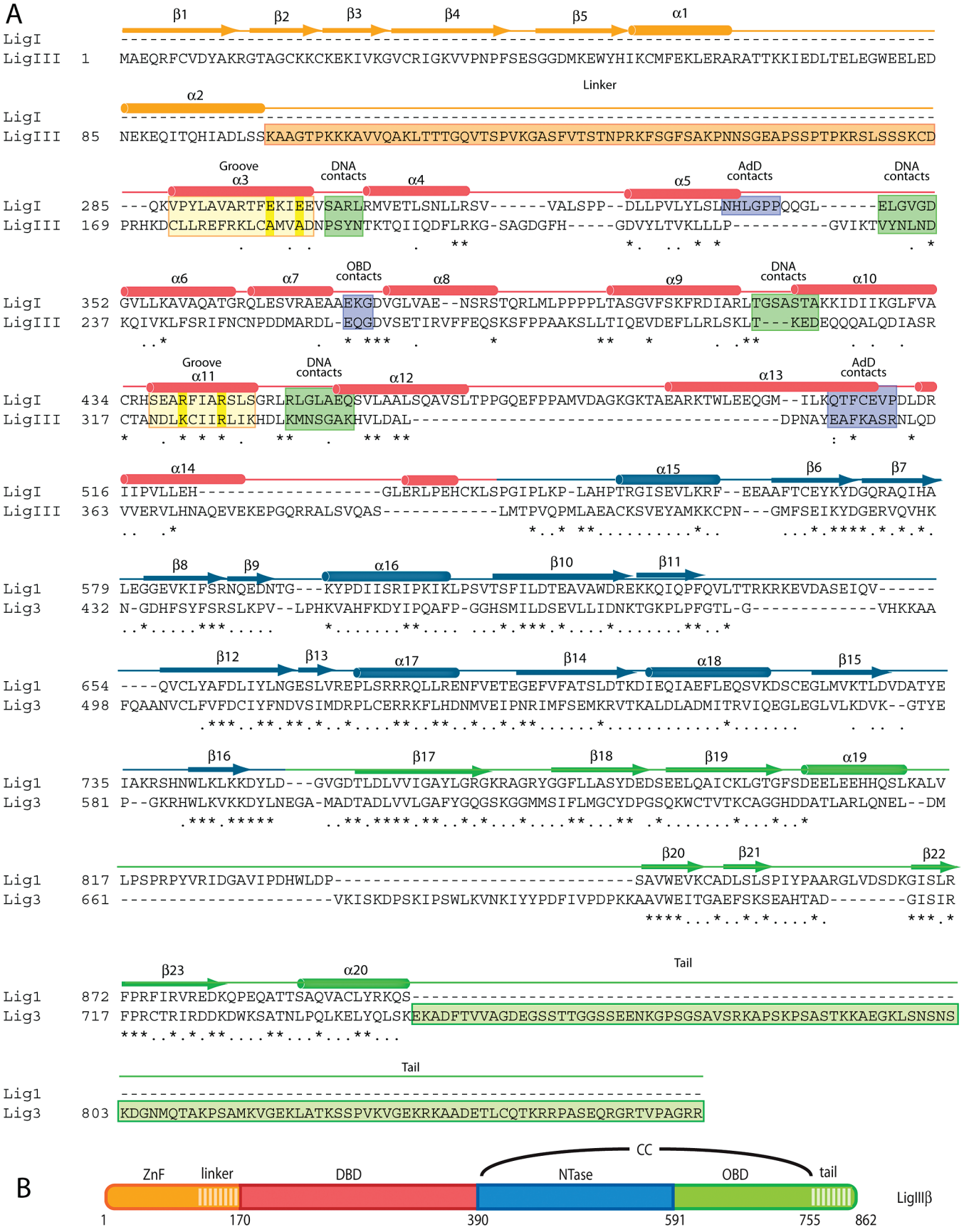

FIGURE 2: Human LigIII structural alignment with human LigI. (A) Structural alignment of LigI and LigIII showing the contrast between the high level of sequence conservation of the NTase and OBD domains and the low level of sequence conservation of the DBD. The secondary structure of LigIII, colored-coded by domain, is indicated above the amino acid sequence. Residues contacting DNA (green) or other domains (purple) are highlighted. The two helices that form a positively charged groove unique to ligase III are highlighted in yellow, with key residues highlighted in bright yellow. (B) Domain structure of ligase III.

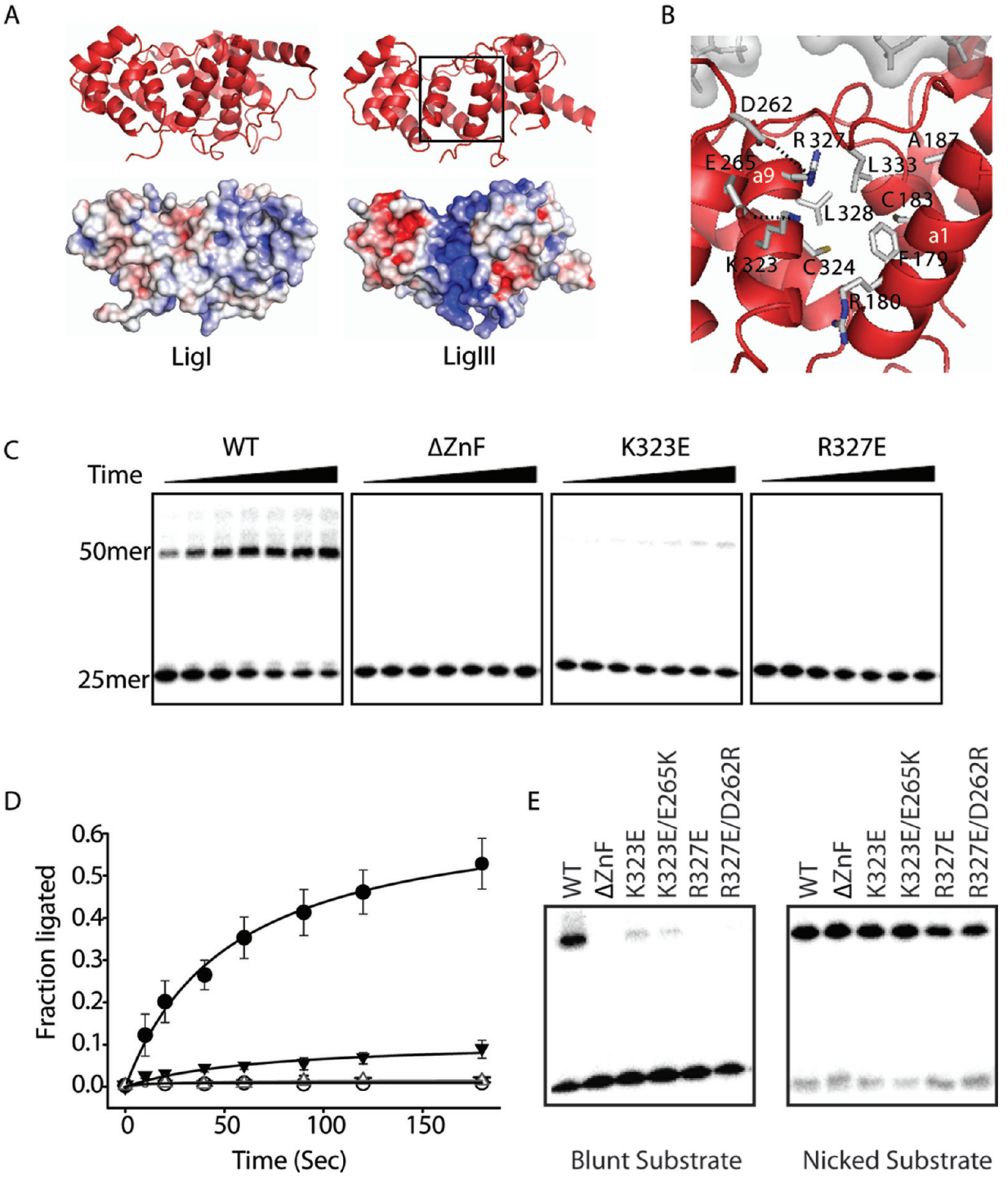

FIGURE 3: Unique positively charged groove in the DBD that is important for intermolecular DNA ligation. (A) Structural comparison of DBDs between ligase I (left) and ligase III reveals a unique positively charged groove of ligase III. (B) Close-up of the positively charged groove, which is boxed in panel A. (C) LigIIIβ, ΔZnF, and two mutants of LigIIIβ (K323E and R327E) with residue substitutions in the positively charged groove were assayed for blunt end joining activity in a single-turnover assay. Proteins (100 nM) were reacted with 4 nM DNA substrates at 22 °C over different periods of time (10 s, 20 s, 40 s, 1 min, 1.5 min, 2 min, and 3 min). (D) Ligated fraction for each protein each protein in panel C: wild type (●), ΔZnF (○), K323E (▼), and R327E (△). Error bars are standard deviations from three separate experiments. (E) Reciprocal charge-reversal mutants (K323E/E265K and R327E/D262R) and their parental single mutants assayed for blunt end and nick joining activity. Proteins (100 nM) were reacted with DNA substrates at 22 °C for 1.5 min.

conformation of LigIII and the post-step 2 conformation of LigI indicate that no change in conformation is required during the step 2 adenylation of the DNA 5′-end.

This new structure of DNA ligase III shows that the DBD is a structurally conserved element of mammalian DNA ligases, despite only 14% sequence identity between the DBDs of LigIII and LigI (Figure 2) (*13*). Not surprisingly, these enzymes have different DNA binding properties (*14*, *15*, *33*, *34*) that may reflect an adaptation of LigIII to its additional ZnF domain. The DBD's α-helical fold has a pseudo-2-fold symmetry (Figure 1C), with each half consisting of a helix−hairpin−helix DNA binding motif and an extended loop that runs along the DNA backbone (Figure 1C). The DNA interaction surface of the DBD covers nearly one and one-half turns of the DNA double helix,

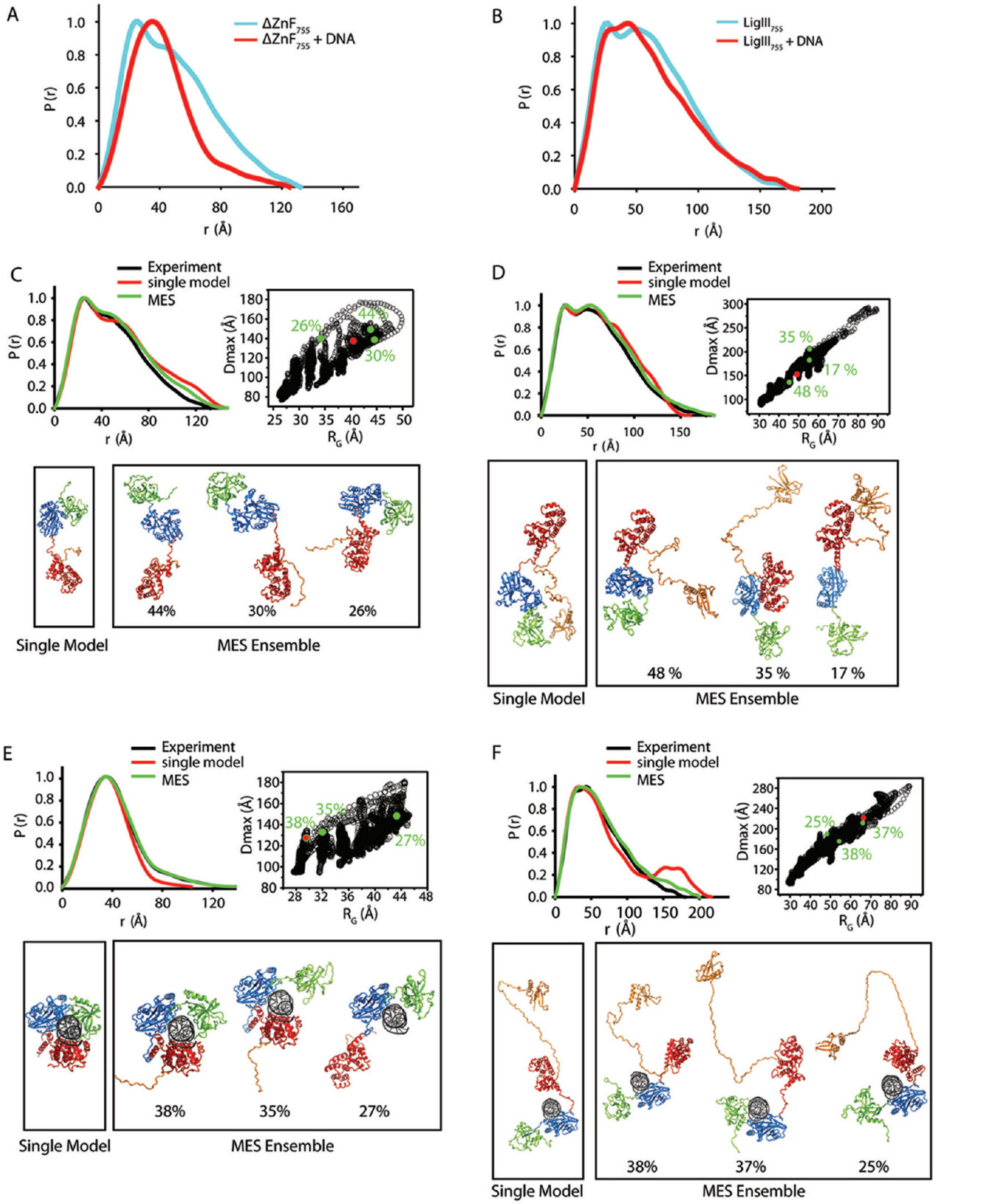

FIGURE 4: Small-angle X-ray scattering of LigIII domains and DNA substrate complexes. (A) Normalized pair distribution [$P(r)$] functions for the ΔZnF_{755} protein in the presence and absence of DNA reveal a large conformational transition of the three conserved domains of LigIII (DBD-NTase-OBD) from an extended to a compact structure. (B) Comparisons of $P(r)$ functions for $LigIII_{755}$ in the presence and absence of DNA show that ZnF-containing LigIII proteins are elongated even when bound to DNA, suggesting that the ZnF adopts flexible conformations during end joining. (C−F) Rigid-body modeling of ΔZnF_{755} (C), $LigIII_{755}$ (D), the ΔZnF_{755}−DNA complex (E), and the $LigIII_{755}$−DNA complex (F) by MD simulation and MES. For each protein complex, the top left panel shows a comparison of the experimental $P(r)$ curve with those calculated from a single best fit model (red) or the MES ensemble (green). In the ΔZnF_{755}−DNA complex (E), the crystal structure of the LigIIIβ ΔZnF−DNA complex is used as the single model. In the top right panel, a comparison of D_{max} values for 10000 models with their R_g values is shown. The best single model and the best fit group of MES conformers are indicated by red and green circles, respectively, with their relative volume fractions. The bottom panels show the single best fit model and three MES conformers with their relative volume fractions. The LigIII domains are colored as in Figure 2.

contacting the DNA backbone and minor groove on the surface opposite the nicked DNA strand. The connecting loops within each helix−hairpin−helix module are inserted into the minor groove where they interact with the edges of base pairs and the DNA phosphates. These interactions are compatible with the underwound structure of the DNA and widened minor groove in complex with LigIII.

The DBD also directly interacts with the NTase and OBD domains, resulting in a closed conformation of LigIII around the DNA nick (Figure 1A). In this conformation, the ZnF is precluded from accessing the nicked DNA strand, implying that the enzyme must adopt a different conformation to enable DNA nick sensing by the ZnF. However, the smaller buried surface area (850 Å^2) at the interface between the DBD and NTase domains of LigIII in comparison to that of LigI [1386 Å^2; Protein Data Bank (PDB) entry 1X9N] may provide greater flexibility to LigIII (Figure S3 of the Supporting Information). This difference in buried surface area is attributed to a short loop in LigIII (residues Pro225−Asn235) that contacts the NTase domain and replaces a longer connecting loop of LigI (residues Asn336−Gly350). We suggest that the smaller, more hydrophilic interface may create a flexible hinge between the DBD and NTase domains of LigIII that facilitates a transition in protein conformation to the closed, catalytic conformation seen in the crystal structure from a nick-sensing conformation that enables the ZnF and DBD to bind cooperatively to DNA (*15*). Further evidence of the conformational flexibility of LigIII is seen in another loop (residues 376−383) that connects the DBD and NTase domains and is disordered in the crystal structure. The SAXS experiments described below provide additional evidence of the flexible structure of DNA ligase III.

Interactions of LigIII with DNA and Nucleotide Substrates. Although the structures of LigIII and LigI in complexes with nicked DNA are similar, these enzymes have significantly different DNA binding activities. LigI binds to DNA with moderate affinity (K_{DNA} = 0.4 μM) but without specificity for nicked DNA. The LigI DBD accounts for most of this binding activity (*14*). LigIII binds to nicked DNA with comparable affinity but relies on the adjacent ZnF domain to supplement the weaker binding affinity of its DBD [K_{DNA} > 20 μM (*15*)]. The DBD of LigIII is designed to function in concert with the ZnF domain, and this domain pair binds tightly and specifically to nicked DNA (K_{DNA} = 0.36 ± 0.06 μM) in a cooperative manner in comparison to either domain in isolation (*15*). In the LigIII crystal structure, the DBD packs against the core NTase and OBD domains and presumably facilitates nick binding by the catalytic core. Thus, the DBD participates in two different modes of nick recognition by LigIII: the catalytic mode of DNA end joining seen in the crystal structure and a nick-sensing mode requiring the enzyme to open so that the ZnF gains access to the DNA ends. The interaction of the LigIII DBD with DNA may coordinate the transition between different DNA binding modes that alternately engage the ZnF and catalytic core. In a comparison of the LigIII and LigI crystal structures, there are differences in the DNA contacts made by their DBDs. Differences in the amino acid sequences of the DNA-contacting loops and their interactions with DNA likely contribute to the higher binding affinity of the LigI DBD.

LigI and LigIII also differ in their activities toward homopolymer substrates (*33*). Specifically, LigIII joins oligo(dT) molecules hybridized to poly(rA), whereas LigI does not (*33*). We previously proposed that the intimate contact of the LigI OBD domain with the minor groove of B-form DNA could explain discrimination against RNA-containing substrates (*14*), and this interaction is conserved in LigIII (Figure S4 of the Supporting Information). We therefore experimentally tested the ability of LigIII to similarly discriminate against RNA-containing polymers of heterogeneous sequence. As predicted from the crystal structure, LigIII discriminates strongly against RNA-containing heteroduplexes, failing to ligate RNA-containing heteroduplexes under conditions that are permissive for DNA ligation (Figure S4B of the Supporting Information, left and center panels). Even under less stringent conditions, at higher temperature and with 25-fold more ligase, LigIII ligates very little of the available RNA-containing substrate after 23 h (< 5% ligated; Figure S4b of the Supporting Information, right panel).

Table 2: Structural Parameters from SAXS Data[a]

	experimental parameters		rigid-body modeling
SAXS sample	D_{max} (Å)	R_g (Å)	χ^2 single model/MES
LigIIIβ	~194	48.5 ± 0.2	
LigIIIβ with DNA	~195	48.4 ± 0.2	
$LigIII_{755}$	~177	45.5 ± 0.2	6.1/3.9
$LigIII_{755}$ with DNA	~180	45.9 ± 0.2	6.3/4.5
ΔZnF	~167	42.9 ± 0.3	
ΔZnF with DNA	~162	40.3 ± 0.2	
ΔZnF_{755}	~132	36.6 ± 0.2	7.3/3.6
ΔZnF_{755} with DNA	~125	31.8 ± 0.1	18.1/3.9
crystal structure of the ΔZnF−DNA complex	~103	28.5 ± 0.2	

[a] R_g is the radius of gyration given by the Guinier approximation (*28*). D_{max} is the maximum protein distance estimated from the $P(r)$ function as shown in Figure 3. χ^2 single model/MES is the goodness of fit χ^2 for the best fit atomic model and multiconformational fit χ^2 for MES models. In the ΔZnF_{755}−DNA complex, χ^2 for single model was calculated from the crystal structure of the ΔZnF−DNA complex.

A Positively Charged Groove in the DBD Supports ZnF Activity. A unique feature on the surface of the DBD from LigIII is a positively charged groove adjacent to the DNA binding surface (Figure 3A). This groove is located at the interface of two halves of the DBD between two parallel helices (α1 and α9), but separated from the DNA binding surface identified in the crystal structure. In the LigI DBD, this groove is absent because the analogous flanking helices have bulky side chains that occupy the groove with uncharged residues (Figure 3A). LigIII helix α9 (residues 318−330) contains two basic residues (Lys323 and Arg327) that are primarily responsible for the positive charge of the groove, whereas the hydrophobic side chains of helix α1 from the other half of the DBD (residues 287−301) participate in forming and stabilizing the groove through hydrophobic interactions with residues of helix α9. The two basic residues (Lys323 and Arg327) are unlikely to contact DNA directly as they located 8.0 and 12.8 Å, respectively from the DNA interface (Figure 3B).

To test the importance of this groove in catalysis, we introduced a series of amino acid substitutions into the DBD of DNA ligase III. The LigIII mutants were assayed for a ZnF-specific activity, the blunt end joining of two DNAs, as well as the nick joining activity that does not require the ZnF. Substitution of either of the positively charged residues in the groove with a glutamate (K323E and R327E) significantly reduced blunt end DNA ligation activity but had very little effect on DNA nick joining activity (Figure 3C,D). We conclude that these mutations do not affect the core activities of LigIII but instead selectively block ZnF function. This effect was quantified by measurement

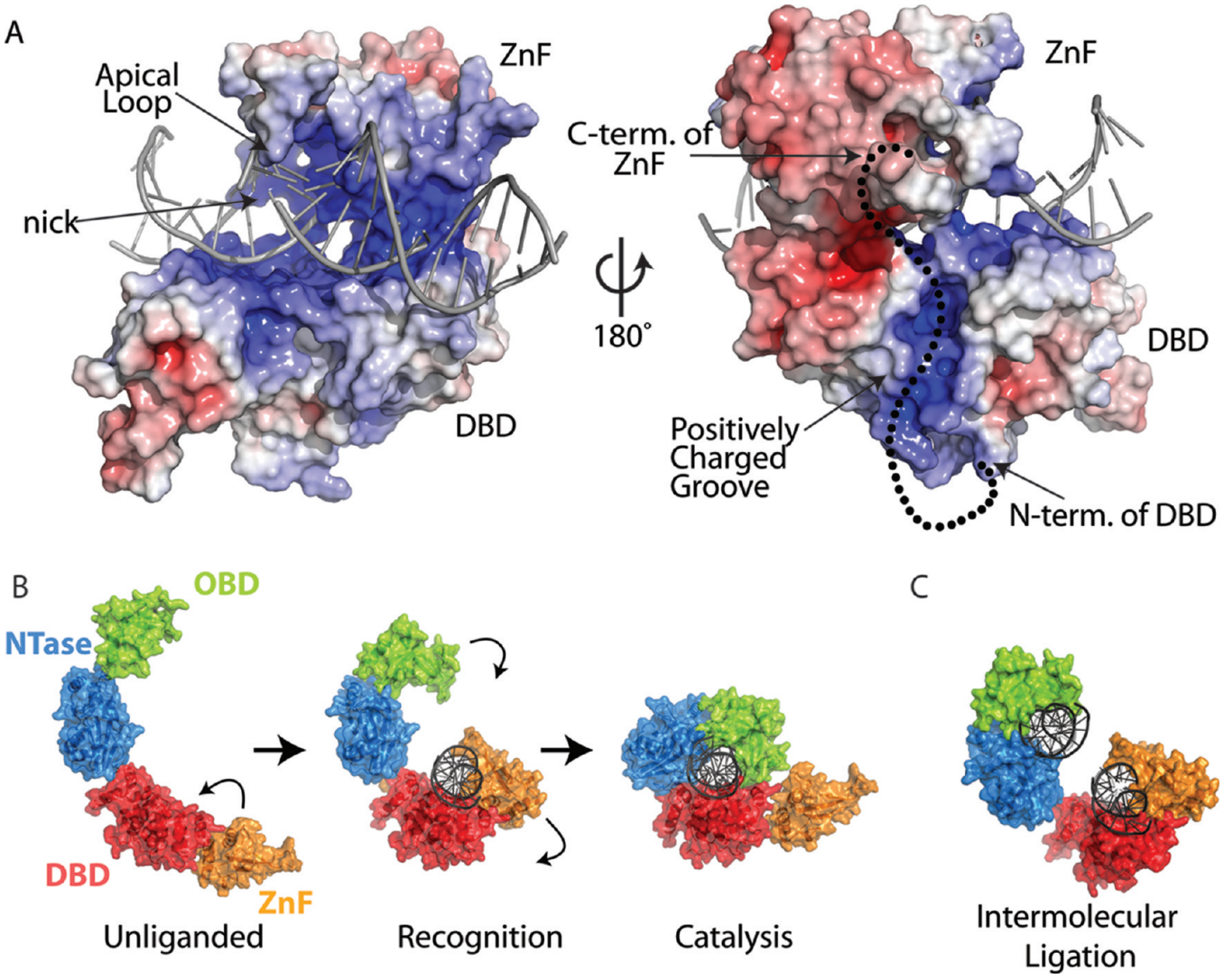

FIGURE 5: Jackknife mechanism of DNA substrate recognition. (A) Model of nick sensing by LigIII. The ZnF solution structure (PDB entry 1uw0) was docked onto the DBD and DNA from the ΔZnF crystal structure to demonstrate how the ZnF DBD module could bind to DNA in a nick sensing mode. Seventy-three residues of ligase III are missing from the two structures used to construct the model. This missing linker between the ZnF and NTase domains may interact with the positively charged groove in the DBD, as indicated by the black dots. (B) Unliganded ligase III adopts an extended conformation, as demonstrated by SAXS experiments. In the substrate recognition step, the ZnF is proposed to insert into the minor groove at the nick, recognizing flexibility in the DNA substrate. In the catalytic step, we hypothesize that the ZnF disengages to allow the DBD, NTase, and OBD domains to fully encircle the nick, resembling the ΔZnF crystal structure. (C) The two DNA binding regions of ligase III (the ZnF-DBD and NTase-OBD) could allow simultaneous binding of two DNAs to stimulate intermolecular ligations.

of the kinetics of ligation by the K323E and R327E mutants (Figure 3C,D). The K323E mutant showed an 87% decrease in the initial velocity of blunt end DNA ligation compared to wild-type LigIII. The R327E mutant is nearly devoid of blunt end joining activity, mimicking a deletion of the ZnF (ΔZnF-LigIII protein). These results suggest an essential role for Arg327 in the function of the ZnF DBD. In contrast, amino acid substitutions of other residues facing the DBD groove (R180E, A187E, and C324Y) had no significant effect on blunt end joining (data not shown).

The substitution of Lys323 and Arg327 with glutamates eliminates the potential for two interhelical salt bridges between α6 and α8 involving the Lys323-Glu265 and Arg327-Asp262 residue pairs, which could destabilize the local structure of the DBD. However, the charge-reversal mutations K323E/E265K and R327E/D262R did not restore efficient blunt end DNA joining activity (Figure 3E). Our results indicate that two basic residues (Lys323 and Arg327) in the DBD of LigIII play critical roles in the ZnF-dependent intermolecular ligation. Given the location of these basic residues, it seems unlikely that they constitute a separate DNA binding site, and we instead propose that the groove containing Lys323 and Arg327 contributes to interdomain interactions between the ZnF and DBD. This interaction could orient the ZnF to participate with the DBD in binding one DNA end while the catalytic core binds a second DNA end to promote blunt end joining (Figure 5).

Conformational Change of LigIII during DNA End Joining. To examine the conformation of DNA ligase III in the presence and absence of a DNA substrate, we performed small-angle X-ray scattering (SAXS) analyses with full-length LigIIIβ and truncated proteins lacking the ZnF [$LigIII_{755}$ and ΔZnF_{755} (Figure 4)]. SAXS provides accurate information about the size and shape of molecules sampled from a population of randomly oriented molecules in solution (*35*, *36*). To simplify the analysis, the C-terminal region that is disordered in the crystal structure (residues 756−820) was also deleted, which resulted in a more compact overall structure but did not change the

interactions with DNA (compare Figure 4 and Figure S5 of the Supporting Information).

The pair distribution functions [$P(r)$] calculated from the SAXS profiles of full-length and truncated versions of LigIIIβ in the absence of DNA have an extended tail (Figure 4A,B) that is consistent with an elongated protein structure (*36*). When complexes with DNA are formed, the $P(r)$ functions are bell-shaped curves that are characteristic of compact globular proteins, particularly for LigIII lacking the ZnF [ΔZnF_{755}−DNA (Figure 4A)]. These observations indicate that LigIII undergoes a large conformational transition that is triggered by binding to DNA, from the elongated unbound protein to a more compact structure in complex with DNA that presumably corresponds to the clamp structure observed in the crystals.

To further test the flexibility and conformational change of the ΔZnF_{755} protein in solution, we used a rigid-body modeling procedure that incorporates molecular dynamics to survey conformational space (*37*). Ten thousand different conformations and their calculated SAXS profiles were generated for ΔZnF_{755} in the presence and absence of DNA, and then a minimal ensemble search (MES) was used to identify the minimal number of conformations required to best fit the experimental data (see Experimental Procedures) (*37*). Combinations of three ΔZnF_{755} conformers with different conformations show better fit (χ^2 = 3.6) than the single best fit model (χ^2 = 7.3), reflecting the flexibility of the ΔZnF_{755} protein in the absence of DNA (Figure 4C and Table 2). For the ΔZnF_{755}−DNA complex, a significantly better fit (χ^2 = 3.9) was obtained for mixtures of three conformers with closed and partially open conformations than for the crystal structure of the ΔZnF−DNA complex (χ^2 = 18.1) (Figure 4E). Thus, in the presence of nicked DNA, the LigIII protein exists in equilibrium between partially open and closed conformations.

Flexible Conformation of the ZnF during End Joining. What is the disposition of the ZnF domain in the closed, catalytically active conformation of LigIIIβ bound to nicked DNA? The $P(r)$ curve of LigIII protein containing the ZnF ($LigIII_{755}$) is indicative of an elongated protein shape, even in the presence of DNA (Figure 4B). Given the dramatic sharpening of the $P(r)$ peak for the ΔZnF_{755}−DNA complex, and the elongated $P(r)$ curve of the $LigIII_{755}$−DNA complex with its significantly larger D_{max} value [~180 Å vs ~125 Å for the ΔZnF_{755}−DNA complex (Table 2)], it appears that the ZnF that does not pack against the DNA and/or other domains of ligase III but instead exists in an extended conformation both in the presence and in the absence of DNA.

To examine the potential flexibility of the ZnF domain, we again used molecular dynamics simulation to sample conformations of $LigIII_{755}$ in the presence and absence of DNA. An ensemble of three conformers of the $LigIII_{755}$ protein with different ZnF conformations improved the fit to the experimental $P(r)$ curve (χ^2 = 3.9) in comparison to the single best fit model (χ^2 = 6.1) (Figure 4D and Table 2). The MES solution (χ^2 = 4.5) for the $LigIII_{755}$−DNA complex is a mixture of open and closed forms of the ΔZnF_{755}−DNA complex, with the ZnF domain highly extended in all selected conformers (Figure 4F). This ensemble accounts for the elongated tail of the experimental $P(r)$ curve with large distances. Thus, the ZnF domain exists in a flexible, elongated conformation that significantly extends the molecular envelope of the LigIII protein both in the presence and in the absence of DNA. The ZnF does not stably bind to DNA when the DBD, OBD, and NTase domains encircle nicked DNA.

DISCUSSION

Mammalian DNA ligases I and III have nonredundant functions in DNA replication and repair, yet these enzymes exhibit remarkably similar structures. There is extensive evidence that protein−protein interactions involving the regions that flank the conserved catalytic region target the three mammalian DNA ligases to different DNA transactions (*38*). In contrast, much less is known about how differences in the catalytic properties of the DNA ligases contribute to their cellular functions. LigI and LigIII have different substrate specificities and DNA binding properties that can be traced to individual domains that constitute these structurally related enzymes. We propose these functional adaptations of LigIII reflect the presence of an N-terminal ZnF that is critical for the participation of ligase III in the repair of single- and double-strand breaks.

The crystal structure of the LigIII−DNA complex supports and extends our knowledge of the core NTase and OBD domains of mammalian ligases that harbor active site residues found in all members of the superfamily of nucleotidyl transferases (*12*). We show that the DBD has a conserved protein fold and mode of interaction with a nicked DNA (Figures 1 and 2), despite the low level of amino acid sequence homology in this region (*13*). The DBD is the common element of two different modes of DNA binding: nick sensing by the ZnF-DBD and catalysis of DNA end joining by the DBD, NTase, and OBD domains (*15*). The switch between these binding modes is likely assisted by the flexible structure of DNA ligase III, which was revealed by small-angle X-ray scattering experiments. The complex of LigIII with DNA in solution shows evidence of multiple conformers (Figure 4), including the closed conformation seen in the crystal structure and partially open conformations that are suggestive of dynamic interactions with the nicked DNA. The DBD may provide an anchoring interaction with DNA that enables flanking domains to exchange on and off the nicked DNA strand without complete dissociation of LigIII from the DNA.

Our biophysical studies show the ZnF does not stably bind to DNA or pack against LigIII when the catalytic domains are clamped around the DNA nick. The ZnF and DBD together constitute an independent DNA end-binding module with supra-additive affinity in comparison to the individual ZnF domain and DBD (*15*). A computational model of the interaction of the ZnF-DBD with DNA (Figure 5) makes the strong prediction that this DNA interaction precludes the nick binding mode revealed by the crystal structure of the catalytic core of LigIII (Figure 1). This model supports the proposed conformational switching between nick sensing and nick sealing modes of DNA engagement that is illustrated by the jackknife model (Figure 5). The ZnF is predicted to bind DNA through a positively charged, concave surface that is made up of a β-sheet, helix 1, and the apical loop connecting β2 to β3 (*17*). We positioned the ZnF so that its positive face contacts the DNA and the apical loop inserts into the minor groove of DNA opposite the nick, in a manner analogous to that of the OBD domain of the ΔZnF-LigIII crystal structure (Figure S2 of the Supporting Information). In this orientation, the ZnF and DBD form a continuous, C-shaped surface that is positively charged and complementary to the underwound DNA from the crystal structure. This docking model places residues in contact with the DNA whose NMR resonances were strongly perturbed by the presence of a nicked DNA (*17*). The apical loop of the ZnF is too wide (8 Å) to fit into the minor groove of B-form DNA (4 Å), but it is accommodated

by the widened minor groove at the site where the OBD binds. The apical loop of the ZnF may therefore serve as a probe for flexible DNA structures that can accommodate a widening of the minor groove. Consistent with this idea, the ZnF of DNA ligase III and similar PARP family zinc fingers bind to irregular structures in DNA, including nicks, single-stranded gaps, and DNA hairpins (*18*, *39*, *40*). The docking model places the C-terminus of the ZnF within 50 Å of the N-terminus of the DBD, a distance readily spanned by the 73-residue linker missing from structures of the ZnF domain and ΔZnF-LigIII protein (Figure 5A). In this position, the ZnF sterically excludes the NTase domain and OBD from binding to DNA. Our studies have identified a unique positively charged groove in the DBD of LigIII, which functionally interacts with the ZnF to promote the ligation of a blunt-ended DNA (Figure 3). We suggest that this groove may provide a docking site that transiently positions the ZnF on DNA during nick sensing (Figure 5B) or during capture of two DNA molecules for intermolecular ligation (Figure 5C).

Although the addition of the purified ZnF *in trans* inhibits DNA joining by ΔZnF-LigIII*β*, the ZnF domain of LigIII*β* enhances nick joining activity, in particular at higher salt concentrations (*15*). To explain this apparent paradox, we proposed a sequential handoff of the DNA from the initial nick sensing by the ZnF-DBD to the engagement of the DNA nick by the catalytic core (*15*). In this model, the flat DNA-binding surface of the DBD acts as a platform that presents the DNA to different domains of ligase III during each step of DNA end joining. This proposed mechanism of ZnF-dependent loading of ligase III onto DNA is named the "jackknife model", which likens LigIII to a pocketknife with multiple domains that have specialized functions during the ligation reaction. The crystal structure and SAXS data clearly demonstrate that the closed conformation of LigIII, with the conserved domains (DBD, NTase, and OBD) encircling the nicked DNA, precludes binding by the ZnF. The jackknife model attempts to reconcile the functional importance of the ZnF for substrate discrimination and catalytic efficiency of LigIII with the apparent transient nature of interactions between the ZnF and the DNA substrate. We suggest that the conformational flexibility of LigIII revealed by SAXS experiments (Figure 4) enables LigIII to efficiently undergo the large-scale, dynamic changes necessary to transition between these two structurally distinct DNA binding modes, nick sensing and nick ligation. This two-step break recognition mechanism is important primarily for DNA breaks that require further processing prior to ligation. Our docking model of the ZnF-DBD bound to DNA suggests that the ZnF might sense DNA flexibility by inserting into the minor groove, enabling selective binding to gaps, flaps, bulges, or double-strand breaks (Figure 5).

Though the requirement for the ZnF in ligation of nicks remains unclear, the ZnF is absolutely required for the intermolecular joining of blunt-ended DNA molecules (*15*). Here we envision that the two DNA binding modules of ligase III, spanning the ZnF-DBD and the NTase-OBD regions (*15*), could bridge between two DNA molecules and align them for ligation by the DBD, NTase, and OBD domains, in a manner analogous to the nick joining reaction depicted by the crystal structure (Figure 5B). This intermolecular joining activity of LigIII is compatible with its involvement in an alternative nonhomologous end joining pathway that repairs DNA double-strand breaks (*2*). Interestingly, this alternative to the dominant, Ku-dependent pathway generates large deletions and chromosomal translocations, genomic rearrangements that are frequently detected in cancer cells (*41*). In addition, cancer cells appear to be more dependent upon this pathway for the repair of DNA double-strand breaks than normal cells (*3*), suggesting that cancer cells will be hypersensitive to inhibitors of backup NHEJ. Our biochemical and biophysical studies delineating the roles of the ZnF and DBD in intermolecular ligation by LigIII provide a rationale for the identification of small molecules that target the ZnF and/or the positively charged groove in the DBD as selective inhibitors of alternative nonhomologous end joining.

Although the core structure of DNA ligase III is based on the same framework as other mammalian ligases, this enzyme has unique adaptations that contribute to the catalytic properties of LigIII, improving the catalytic efficiency of DNA single-strand break repair and enabling efficient ligation of two blunt-ended DNAs (*15*). These distinctive DNA binding and enzymatic properties of ligase III contribute to its biological specialization, in addition to protein−protein interactions that target the enzyme to sites of DNA damage. Alternative modes of DNA interaction may also contribute to the fidelity of DNA end joining and provide opportunities for regulation of ligation activity to prevent the formation of dead end intermediates that inhibit repair of the break (*42*). The flexible structure of ligase III may facilitate recruitment to single-strand breaks while leaving the DNA accessible to other modifying enzymes for a sequential handoff of repair intermediates that promotes efficient repair of DNA damage while preventing toxic or mutagenic outcomes. Understanding these biologically important handoffs, which may also be critical for base excision repair (*43*, *44*), will require the integration of structural models of conformational change with the rates and mechanisms of enzymatic functions, as developed here for DNA ligase III using crystallography, SAXS, and mutational analyses.

ACKNOWLEDGMENT

John Pascal kindly provided us with RNA substrates.

SUPPORTING INFORMATION AVAILABLE

Additional figures and experimental procedures. This material is available free of charge via the Internet at http://pubs.acs.org.

REFERENCES

1. Tomkinson, A. E., Vijayakumar, S., Pascal, J. M., and Ellenberger, T. (2006) DNA ligases: Structure, reaction mechanism, and function. *Chem. Rev. 106*, 687–699.
2. Wang, H., Rosidi, B., Perrault, R., Wang, M., Zhang, L., Windhofer, F., and Iliakis, G. (2005) DNA ligase III as a candidate component of backup pathways of nonhomologous end joining. *Cancer Res. 65*, 4020–4030.
3. Sallmyr, A., Tomkinson, A. E., and Rassool, F. V. (2008) Up-regulation of WRN and DNA ligase IIIα in chronic myeloid leukemia: Consequences for the repair of DNA double-strand breaks. *Blood 112*, 1413–1423.
4. Puebla-Osorio, N., Lacey, D. B., Alt, F. W., and Zhu, C. (2006) Early embryonic lethality due to targeted inactivation of DNA ligase III. *Mol. Cell. Biol. 26*, 3935–3941.
5. Dulic, A., Bates, P. A., Zhang, X., Martin, S. R., Freemont, P. S., Lindahl, T., and Barnes, D. E. (2001) BRCT domain interactions in the heterodimeric DNA repair protein XRCC1-DNA ligase III. *Biochemistry 40*, 5906–5913.
6. Nash, R. A., Caldecott, K. W., Barnes, D. E., and Lindahl, T. (1997) XRCC1 protein interacts with one of two distinct forms of DNA ligase III. *Biochemistry 36*, 5207–5211.
7. Mackey, Z. B., Ramos, W., Levin, D. S., Walter, C. A., McCarrey, J. R., and Tomkinson, A. E. (1997) An alternative splicing event which occurs in mouse pachytene spermatocytes generates a form of

DNA ligase III with distinct biochemical properties that may function in meiotic recombination. *Mol. Cell. Biol. 17*, 989–998.
8. Husain, I., Tomkinson, A. E., Burkhart, W. A., Moyer, M. B., Ramos, W., Mackey, Z. B., Besterman, J. M., and Chen, J. (1995) Purification and characterization of DNA ligase III from bovine testes. Homology with DNA ligase II and vaccinia DNA ligase. *J. Biol. Chem. 270*, 9683–9690.
9. Lakshmipathy, U., and Campbell, C. (2000) Mitochondrial DNA ligase III function is independent of Xrcc1. *Nucleic Acids Res. 28*, 3880–3886.
10. Lakshmipathy, U., and Campbell, C. (1999) The human DNA ligase III gene encodes nuclear and mitochondrial proteins. *Mol. Cell. Biol. 19*, 3869–3876.
11. McKinnon, P. J., and Caldecott, K. W. (2007) DNA strand break repair and human genetic disease. *Annu. Rev. Genomics Hum. Genet. 8*, 37–55.
12. Shuman, S., and Schwer, B. (1995) RNA capping enzyme and DNA ligase: A superfamily of covalent nucleotidyl transferases. *Mol. Microbiol. 17*, 405–410.
13. Martin, I. V., and MacNeill, S. A. (2002) ATP-dependent DNA ligases. *Genome Biol. 3*, No. REVIEWS3005.
14. Pascal, J. M., O'Brien, P. J., Tomkinson, A. E., and Ellenberger, T. (2004) Human DNA ligase I completely encircles and partially unwinds nicked DNA. *Nature 432*, 473–478.
15. Cotner-Gohara, E., Kim, I. K., Tomkinson, A. E., and Ellenberger, T. (2008) Two DNA-binding and nick recognition modules in human DNA ligase III. *J. Biol. Chem. 283*, 10764–10772.
16. Mackey, Z. B., Niedergang, C., Murcia, J. M., Leppard, J., Au, K., Chen, J., de Murcia, G., and Tomkinson, A. E. (1999) DNA ligase III is recruited to DNA strand breaks by a zinc finger motif homologous to that of poly(ADP-ribose) polymerase. Identification of two functionally distinct DNA binding regions within DNA ligase III. *J. Biol. Chem. 274*, 21679–21687.
17. Kulczyk, A. W., Yang, J. C., and Neuhaus, D. (2004) Solution structure and DNA binding of the zinc-finger domain from DNA ligase IIIα. *J. Mol. Biol. 341*, 723–738.
18. Taylor, R. M., Whitehouse, C. J., and Caldecott, K. W. (2000) The DNA ligase III zinc finger stimulates binding to DNA secondary structure and promotes end joining. *Nucleic Acids Res. 28*, 3558–3563.
19. Van Duyne, G. D., Standaert, R. F., Karplus, P. A., Schreiber, S. L., and Clardy, J. (1993) Atomic structures of the human immunophilin FKBP-12 complexes with FK506 and rapamycin. *J. Mol. Biol. 229*, 105–124.
20. Otwinowski, Z., and Minor, W. (1997) Processing of X-ray Diffraction Data Collected in Oscillation Mode. *Methods Enzymol. 276*, 307–326.
21. Pflugrath, J. W. (1999) The finer things in X-ray diffraction data collection. *Acta Crystallogr. 55*, 1718–1725.
22. Terwilliger, T. C., and Berendzen, J. (1999) Automated MAD and MIR structure solution. *Acta Crystallogr. 55*, 849–861.
23. de La Fortelle, E., Bricogne, G., and Carter, C. W., Jr. (1997) Maximum-likelihood heavy-atom parameter refinement for multiple isomorphous replacement and multiwavelength anomalous diffraction methods. In Methods in Enzymology, pp 472−494, Academic Press, San Diego.
24. Emsley, P., and Cowtan, K. (2004) Coot: Model-building tools for molecular graphics. *Acta Crystallogr. 60*, 2126–2132.
25. Murshudov, G. N., Vagin, A. A., and Dodson, E. J. (1997) Refinement of macromolecular structures by the maximum-likelihood method. *Acta Crystallogr. 53*, 240–255.
26. Baker, N. A., Sept, D., Joseph, S., Holst, M. J., and McCammon, J. A. (2001) Electrostatics of nanosystems: Application to microtubules and the ribosome. *Proc. Natl. Acad. Sci. U.S.A. 98*, 10037–10041.
27. Hura, G. L., Menon, A. L., Hammel, M., Rambo, R. P., Poole, F. L., II, Tsutakawa, S. E., Jenney, F. E., Jr., Classen, S., Frankel, K. A., Hopkins, R. C., Yang, S. J., Scott, J. W., Dillard, B. D., Adams, M. W., and Tainer, J. A. (2009) Robust, high-throughput solution structural analyses by small angle X-ray scattering (SAXS). *Nat. Methods 6*, 606–612.
28. Guinier, A., and Fournet, F. (1955) Small Angle Scattering of X-rays, Wiley Interscience, New York.
29. Svergun, D. (1992) Determination of the regularization parameter in indirect-transform methods using perceptual criteria. *J. Appl. Crystallogr. 25*, 495–503.
30. Pelikan, M., Hura, G. L., and Hammel, M. (2009) Structure and flexibility within proteins as identified through small angle X-ray scattering. *Gen. Physiol. Biophys. 28*, 174–189.
31. Nandakumar, J., Nair, P. A., and Shuman, S. (2007) Last stop on the road to repair: Structure of *E. coli* DNA ligase bound to nicked DNA-adenylate. *Mol. Cell 26*, 257–271.
32. Nair, P. A., Nandakumar, J., Smith, P., Odell, M., Lima, C. D., and Shuman, S. (2007) Structural basis for nick recognition by a minimal pluripotent DNA ligase. *Nat. Struct. Mol. Biol. 14*, 770–778.
33. Tomkinson, A. E., Roberts, E., Daly, G., Totty, N. F., and Lindahl, T. (1991) Three distinct DNA ligases in mammalian cells. *J. Biol. Chem. 266*, 21728–21735.
34. Bhagwat, A. S., Sanderson, R. J., and Lindahl, T. (1999) Delayed DNA joining at 3′ mismatches by human DNA ligases. *Nucleic Acids Res. 27*, 4028–4033.
35. Koch, M. H., Vachette, P., and Svergun, D. I. (2003) Small-angle scattering: A view on the properties, structures and structural changes of biological macromolecules in solution. *Q. Rev. Biophys. 36*, 147–227.
36. Putnam, C. D., Hammel, M., Hura, G. L., and Tainer, J. A. (2007) X-ray solution scattering (SAXS) combined with crystallography and computation: Defining accurate macromolecular structures, conformations and assemblies in solution. *Q. Rev. Biophys. 40*, 191–285.
37. Pelikan, M., Hura, G. L., and Hammel, M. (2009) Structure and flexibility within proteins as identified through small angle X-ray scattering. *Gen. Physiol. Biophys. 28*, 174–189.
38. Ellenberger, T., and Tomkinson, A. E. (2008) Eukaryotic DNA ligases: Structural and functional insights. *Annu. Rev. Biochem. 77*, 313–338.
39. Petrucco, S. (2003) Sensing DNA damage by PARP-like fingers. *Nucleic Acids Res. 31*, 6689–6699.
40. Petrucco, S., Volpi, G., Bolchi, A., Rivetti, C., and Ottonello, S. (2002) A nick-sensing DNA 3′-repair enzyme from *Arabidopsis*. *J. Biol. Chem. 277*, 23675–23683.
41. Wang, H., Perrault, A. R., Takeda, Y., Qin, W., Wang, H., and Iliakis, G. (2003) Biochemical evidence for Ku-independent backup pathways of NHEJ. *Nucleic Acids Res. 31*, 5377–5388.
42. Ahel, I., Rass, U., El-Khamisy, S. F., Katyal, S., Clements, P. M., McKinnon, P. J., Caldecott, K. W., and West, S. C. (2006) The neurodegenerative disease protein aprataxin resolves abortive DNA ligation intermediates. *Nature 443*, 713–716.
43. Garcin, E. D., Hosfield, D. J., Desai, S. A., Haas, B. J., Bjoras, M., Cunningham, R. P., and Tainer, J. A. (2008) DNA apurinic-apyrimidinic site binding and excision by endonuclease IV. *Nat. Struct. Mol. Biol. 15*, 515–522.
44. Parikh, S. S., Putnam, C. D., and Tainer, J. A. (2000) Lessons learned from structural results on uracil-DNA glycosylase. *Mutat. Res. 460*, 183–199.
45. Ciarrocchi, G., Lestingi, M., Wright, G., and Montecucco, A. (1993) Bacteriophage T4 and human type I DNA ligases relax DNA under joining conditions. *Nucleic Acids Res. 21*, 5934–5939.